1
2
Injectable, strong and bioadhesive catechol-chitosan hydrogels physically crosslinked using sodium bicarbonate

3   Capucine Guyot[a,b], Marta Cerruti[c] and Sophie Lerouge[a,b,*]

4   capucine.guyot.1@etsmtl.ca
5   marta.cerruti@mcgill.ca
6   sophie.lerouge@etsmtl.ca (corresponding author), +15143968836

7   [a]Dept of Mechanical Engineering, École de Technologie Supérieure, 1100 rue Notre-Dame Ouest,
8   Montréal QC H3C 1K3 Canada.

9   [b]Centre de Recherche du CHUM, 900 Rue Saint-Denis, Montréal, QC H2X 0A9 Canada.

10 [c]Dept of Materials Engineering, McGill University, 3610 Rue University, Montréal QC H3A 0C5 Canada

11 ## Abstract

12 Fast-gelling chitosan thermosensitive hydrogels have proven to be excellent matrices for targeted
13 drug-delivery and cell therapy. In this work, we demonstrate the possibility of designing injectable
14 bioadhesive hydrogels with a high gelation rate by modifying chitosan with catechol (cat-CH) and
15 using sodium bicarbonate (SHC) as a gelling agent. Cat-CH/SHC hydrogels gel under five minutes
16 at 37 °C and reach a high secant modulus after 24h (E=90 kPa at 50% strain). Besides, they show
17 significantly higher adhesion to tissues than chitosan hydrogels thanks to the combination of
18 catechol grafting and physical crosslinking. Their pH and osmolality stayed inside the physiological
19 range. While biocompability tests will be mandatory to conclude regarding their potential for drug
20 of cell encapsulation, these hydrogels uniquely combine physiological compatibility, injectability,
21 fast gelation, good cohesion, and bioadhesion.

22 ## Keywords

23 Biomaterials; hydrogels; chitosan; biomimetism; catechol; bioadhesion;

24 ## 1. Introduction

25 Systemic delivery of active compounds such as drugs or cells suffers from several drawbacks, such
26 as a limited therapeutic efficacy and possible adverse effects due to the dispersion in non-targeted
27 tissues. There is a need for a local and sustained delivery directly at the target site by trapping the
28 bioactive compounds into matrices and leaching them over time. Ideally, those matrices should be
29 injectable, an asset that strongly simplifies surgical procedures and reduces post-operative
30 complications [1]. Hydrogels are particularly interesting since those polymeric 3D structures can
31 retain large amounts of water and mimic the viscoelastic properties of the extracellular matrix. They
32 are already widely used as drug or cell carriers [2] for various biomedical applications. Nonetheless,
33 they generally lack bioadhesion, i.e., the ability to bind to target tissues through either chemical
34 (covalent) or strong physical (supramolecular) interactions [3]. Bioadhesion prevents unwanted
35 detachment and favours drug or cell paracrine factors transfer to the target tissues [3,4]. Good
36 bioadhesion requires the synergy between a strong hydrogel/tissue interface and a good cohesion
37 of the hydrogel itself to prevent mechanical failure [5].

38 Chitosan (CH) is an excellent biopolymer for many biomedical applications thanks to its
39 biocompatibility and biodegradability [6]. CH is soluble in its cationic form (pH <6.3), which
40 makes it moderately bioadhesive thanks to electrostatic interactions [7]. When combined with a
41 weak base in the right proportions, CH forms strong and cell-compatible hydrogels thanks to their
42 neutral pH and mild crosslinking conditions, without any toxic chemical crosslinker. Moreover,
43 these hydrogels are thermosensitive; they are liquid at room temperature, which makes it easy to

44 mix them with cells and to inject them through small needles and catheter, and they autonomously
45 gel at body temperature.

46 The first CH-based thermosensitive hydrogel used glycerophosphate (GP) [8]. CH/GP hydrogels
47 gel at 37 °C, usually reaching a soft consistency in less than five minutes [9]. However, their high
48 osmolality (a consequence of the high GP concentration) causes osmotic stress, resulting in a high
49 death rate of encapsulated cells [10,11]. GP can be substituted by another alkaline compound which
50 pKa is the same as the pKa of chitosan at room temperature [12]. A good candidate is sodium
51 bicarbonate (sodium hydrogen carbonate, herein abbreviated SHC) [13], because its pKa is 6.33
52 regardless of temperature. The gelation mechanism of CH/SHC hydrogels resembles the gelation
53 mechanism of CH/GP hydrogels described by Lavertu et al. [12]. At room temperature, SHC
54 screens the NH_3^+ of chitosan. When the temperature increases, the pKa of chitosan decreases; SHC
55 reacts with NH_3^+ and is released as CO_2 (as described in Eq.(1)). The stability at room temperature
56 avoids electrostatic repulsion between the CH chains, bringing them close to one another so that
57 they irrevocably set into a 3D network when SHC escapes. CH/SHC hydrogels show significantly
58 lower osmolality and higher secant modulus than CH/GP hydrogels [14]. Yet, since the amino
59 groups of CH are neutralized during gelation, CH is no longer cationic and these hydrogels show
60 no significant adhesion to tissues.

$$chitosanNH_3^+ + HCO_3^- \longrightarrow chitosanNH_2 + H_2O + CO_2 \nearrow \qquad (1)$$
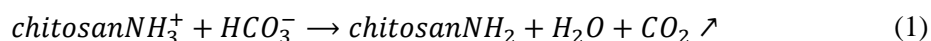
61 To improve the mild bioadhesive properties of CH, several research groups looked into the amino
62 acid 3.4-dihydroxyphenylalanine (DOPA), which is especially prevalent in the marine mussel's
63 feet [15]. DOPA contains catechol (cat), a diphenol that is responsible for most of the mussel's
64 incredible adhesion underwater [16]. Since this discovery, researchers have grafted catechol-
65 bearing molecules to different polymers [17–19], including CH [20], significantly improving their
66 bioadhesiveness [21,22]. Cat is known to be adhesive to both inorganic and organic substrates.
67 Adhesion to inorganic surfaces is attributed to physical bonding through electronic, hydrophobic
68 and π-π interactions [23]. In a pro-oxidative environment and at pH7 and above, cat groups oxidize
69 into quinones [24] which subsequently react with amino groups [25] to form covalent bonds
70 (Figure 1). Hence, oxidized cat strongly adheres to aminated organic surfaces [5,26,27]. However,
71 catechol-chitosan (cat-CH) also bears amino groups. This can result in covalent self-crosslinking,
72 referred to as oxidative crosslinking in this paper, a slow process that leads to soft hydrogels [28].
73 Moreover, since a fraction of the cat groups is wasted to maintain the network cohesion, so-formed
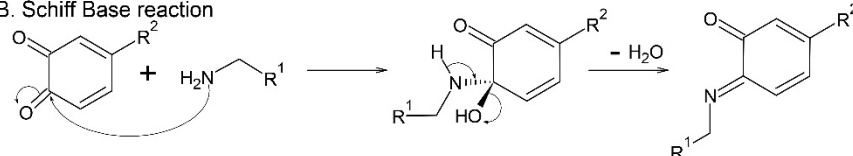74 hydrogels are less bioadhesive.

75
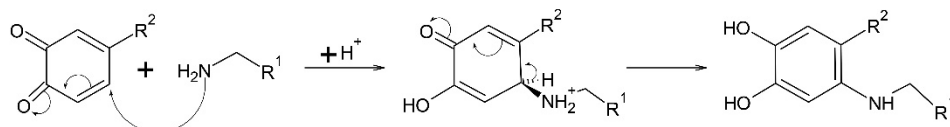
76 Figure 1: Two potential mechanisms for the formation of a covalent bond between quinones and amines.

77 In this work, we explored the combination of cat-CH and SHC in the design of physical bioadhesive
78 hydrogels that are thermosensitive, injectable, and can reach a high level of mechanical cohesion.

79   Given that the pH of CH/SHC hydrogels is above 7 [29], catechol groups in cat-CH/SHC hydrogels
80   should (at least partially) oxidize. Our main working hypothesis is that by using SHC, cat-CH will
81   physically crosslink quickly enough to limit oxidative crosslinking to a great extent, leading to an
82   improvement in both mechanical properties and bioadhesive properties. We showed how, by tuning
83   the SHC concentration, we can optimize the stiffness, gelation temperature (below 37°C to allow
84   for injection), gelation rate and pH of hydrogels.

85   We also tried as a working side hypothesis to prevent oxidation altogether by dissolving cat-CH in
86   acidic conditions instead of water. This can avoid catechol-to-quinone oxidation during hydrogel
87   preparation. Moreover, decreasing the pH could also increase the ionization level of CH, i.e., the
88   ratio of NH_3^+ versus NH_2. With more charge screening we expect a neater organization of the chains
89   with one another followed by a slower and more homogeneous deionization of CH with increasing
90   temperature, translating to an increase in mechanical properties after gelation.

91   2.   Experimental

92   2.1. Cat-CH preparation and characterization

93   2.1.1.   Reagents

94   Chitosan (CH, ChitoClear®; M_w = 150–250 kDa [mean], DDA = 80% measured by NMR using a
95   previously established protocol [30]) was obtained from Primex (Island). Hydrocaffeic acid (HCA)
96   and 1-Ethyl-3- (3-dimethylaminopropylcarbodiimide (EDC) were purchased from Sigma-Aldrich
97   (USA). Dialysis membrane (Spectra/Por®7, MWCO = 3.5 kDa) was from Spectrum Laboratories
98   Inc. (USA). Sodium hydrogen carbonate (SHC) was from E.M.D. Millipore (Germany).

99   2.1.2.   Cat-CH Synthesis

100 HCA, a molecule that bears a catechol group, was grafted onto CH by a carbodiimide coupling
101 reaction (see Figure 2). CH was dissolved at 0.1% w/v in 50 mM HCl (pH=2.5) to ensure its
102 complete ionization. HCA was dissolved in ethanol (EtOH) at 0.025% w/v. EDC was dissolved in
103 water at different concentrations to modulate reagents molar ratio (between 1:1:1 and 1:1:2
104 CH:HCA:EDC, see Figure A. 1. Both were added to the CH solution under controlled mixing
105 speed, either 300 rpm or 750 rpm. To avoid catechol oxidation, we equilibrated the pH at 4.8 with
106 0.5 M NaOH before leaving the reaction overnight. Cat-CH was then purified by dialysis against
107 pH2 10 mM NaCl for two days followed by deionized water (DW) for six hours. Finally, cat-CH
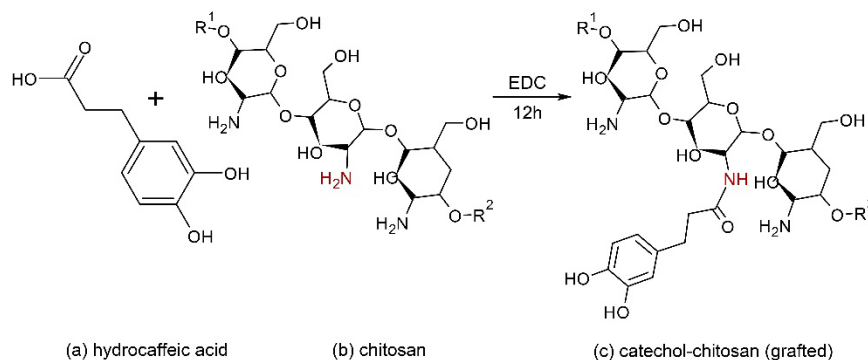108 was freeze-dried and stored at room temperature.

(a) hydrocaffeic acid   (b) chitosan   (c) catechol-chitosan (grafted)

110   Figure 2: Carbodiimide coupling reaction between CH and HCA

2.1.3. Chemical characterization

NMR[1]H (Varian VNMRS 500 MHz, Montréal) was performed on CH and cat-CH 0.1% w/v solutions in DCl. A signal between 6.5 ppm and 6.7 ppm confirmed the success of the cat grafting [31]. UV-visible spectrometry (Cary5000 Agilent, Montréal) was then used to quantify catechol grafting. We first established a calibration curve at 280 nm for HCA using standard solutions (0.1 mM to 0.5 mM)). Cat-CH was then dissolved in water at 0.05% (w/v). We measured its absorbance and related it to catechol concentration in the sample thanks to the calibration curve. The relationship between catechol concentration and catechol grafting degree (χ, expressed in % of the total molar number of monomers, see Eq.A-1). For the rest of the paper, cat-CH will be referred to as catχ-CH, where χ corresponds to the catechol grafting degree of each sample.

2.1.4. pKa assessment

Cat-CH was dissolved in water or 50 mM HCl at 0.1% (w/v) and titrated with 0.1M, 0.5M or 2M NaOH depending on the required precision. The pH was monitored with a Denver Instrument pH meter. pKa was assessed at half-equivalence with Eq.(2) (n_{eq} being the amount of NaOH at equivalence).

$$pK_A = pH(\frac{n_{eq}}{2}) \tag{2}$$

2.2. Synthesis and characterization of hydrogels

2.2.1. Preparation of hydrogels

Cat-CH (3.33% w/v) was dissolved in either deionized water (H_2O) or acid excess (50 mM HCl). Cat-CH hydrogels were prepared by mixing cat-CH with SHC solutions at a 3:2 volumetric ratio. Cat-CH concentration in the gel was therefore 2% (w/v), HCl concentration was 30 mM, and SHC concentration ranged from 50 mM to 130 mM (abbreviated SHCn, n being the SHC concentration in mM). Unmodified CH hydrogels (2% w/v) were made by mixing 3.33% (w/v) CH dissolved in 90 mM HCl with 175 mM SHC. Occurrence of oxidation for cat-CH solutions and cat-CH hydrogels was noticeable by a change in colour from white to orange.

2.2.2. Mechanical Tests

The gelation kinetics of all hydrogels were tested on a Physica MCR301 rheometer (Anton Paar) directly after mixing using a concentric cylinder geometry (CC10). Their gelation temperature was assessed by performing a temperature ramp, while gelation time was assessed by a time sweep at a chosen temperature. For the temperature ramps, temperature was initially set to 5 °C and increased by 1°C/minute until it reached 65 °C. Temperature ramps were performed to confirm that gelation is triggered at a temperature between 22°C and 37°C. For the time sweep assays, temperature was first set to 22°C, and suddenly increased after 1 minute to either 37°C or 50°C for one hour. Time sweeps at 37°C mimicked in-vivo injection. Time sweeps at 50°C were less relevant for biomedical applications but were performed to get a better understanding of the differences between the formulations. All experiments were performed in the linear viscoelastic region at 5% strain and 1 Hz frequency. In addition, to study the rheological behaviour at 22°C and demonstrate injectability, dynamic viscosity as a function of shear rate (0.1 s-1 to 200 s-1) was acquired on a plate/plate geometry. Some formulations were submitted to extrusion through a 25G needle.

Compression tests were performed on an Electroforce 3,200 (TA Instruments). Pre-gel solutions were poured into 7 mm cylindrical moulds and allowed to gel at 37°C for 24 hours to ensure that all gels had enough time to reach their final mechanical properties. The displacement rate was calculated based on the sample height to achieve 100% deformation/minute. Compression was applied until 50% deformation and stress was calculated based on the recorded resulting force and

154 the sample section. Since the hydrogel presents a non-linear elastic behaviour, the stiffness
155 (Young's modulus E) is strain dependent. Therefore, the stiffness was characterized by the secant
156 moduli, i.e the slope of a line connecting the point of zero strain (ε_0) to a point at a specified
157 deformation (ε) as described by Eq.(3).

$$E_\varepsilon = \frac{\sigma_\varepsilon - \sigma_{\varepsilon_0}}{\varepsilon} \qquad (3)$$

158 ### *2.2.3. pH and osmolality*

159 We measured the pH of cat-CH/SHC hydrogels right after mixing and after 24 hours of gelation
160 using a Laquatwin pH-22 electrode (HORIBA, Japan). Osmolality was measured on hydrogel
161 filtrates using an Advanced Micro Osmometer 3,300 (Advanced Instruments) as described in [10].
162 Measures were performed in triplicate.

163 ### *2.2.4. Adhesive Tests*

164 Adhesion on inorganic substrates (SiO2) was evaluated quantitatively on an Electroforce 3,200
165 instrument (Bose Corporation, USA). A thin layer of cat-CH or cat-CH/SHC solution was spread
166 at room temperature between two glass slides, leaving a few centimetres free on top for clamping.
167 All samples were incubated at 37 °C for 24h to ensure that the gels had reached their final
168 mechanical properties. A moist environment was recreated in the sample holders to simulate
169 adhesion occurring in wet conditions. Slides were then mounted on clamps, one static and one
170 pulling upwards to generate shear stress. We recorded the maximum detachment and noticed
171 whether the glass/gel interface or the core of the hydrogel broke first. The maximum detachment
172 shear was then calculated by dividing the maximal detachment force by the sample surface.

173 Bioadhesion was evaluated qualitatively by a wash-off test modified from [32]. Porcine intestinal
174 tissue was harvested from pigs sacrificed in the framework of other studies and kept at +4 °C in
175 PBS 10% v/v for a maximum of 5 hours before use. Animal surgical procedures were approved by
176 the institutional animal care committee at the CRCHUM and the Canadian Council on Animal
177 Care. The tissue was washed right before the experiment, cut open and sliced into rectangles
178 (25 mm × 56 mm), before being glued to glass slides with cyanoacrylate (Vetbond, 3M Animal
179 Care Products, Japan). The first five centimetres of the slide were kept free to allow for sample
180 clamping. Cat3-CH/SHC or CH/SHC solutions were poured into cylindrical moulds directly on the
181 tissue. We incubated at 37 °C in a moist environment and the moulds were removed after 24h. The
182 slides were clipped onto a rotating arm and immersed into a 37 °C PBS bath. The rotating speed
183 was controlled by a potentiometer and increased by 25 rpm every 5 minutes. We recorded the
184 number of detached hydrogels samples every five minutes.

185 ### *2.2.5. Statistical Analysis*

186 Statistical analysis was executed on Graphpad Prism. For single parameter analysis, we performed
187 t-tests and expressed significance through resulting p-values. $p < 0.05$ was considered a low
188 significance (*), $p < 0.005$ was considered a high significance (***). For two-parameter analysis,
189 we performed two-way ANOVA followed by a Tukey post-test.

190 ## 3. Results and discussion

191 ## 3.1. Cat-CH polymer

192 ### *3.1.1. Cat-CH grafting*

193 We first confirmed the grafting of cat on chitosan based on the NMR spectra (Figure A. 2). Unlike
194 CH solutions, a distinctive signal was noticeable in the 6.5-6.7 ppm range corresponding to the
195 aromatic protons of the catechols. UV-visible spectrometry was then used to quantify the amount

196 of grafted catechol. Cat was grafted to CH using four ratios of HCA/EDC and two mixing speeds.
197 As seen on Figure A. 1, both parameters influenced χ (cat grafting degree), which ranged from 4%
198 (slow mixing, 1/1 ratio) to 23% (rapid mixing, 1/2 ratio). Introducing an excess of EDC and using
199 a high-mixing speed were synergistic to increase the probability of having interactions between
200 NH_3^+ and HCA. Our cat grafting degrees were similar to those of previous authors, who reported
201 values ranging between 3.3% and 20.5% [21,22,28,31,33–36]. Nonetheless, as we noticed from the
202 standard deviation, the higher the yield and the more variability between the samples. As a result,
203 in the paper we report χ for each specific batch of cat-CH.

3.1.2. pKa of cat-CH

205 As explained in the introduction, the pKas of chitosan and SHC must be the same to achieve
206 physical gelation. To ensure that cat grafting did not significantly affect the pKa of chitosan, the
207 pKas of cat3-CH and cat23-CH were assessed by titration. Cat3-CH and cat23-CH were dissolved
208 in either water or HCl (further respectively abbreviated cat-CH H_2O and cat-CH HCl). CH (control)
209 was only soluble in HCl. All the solutions were titrated against NaOH.

210 The titration curves of cat-CH HCl (Figure 3A) and CH (Figure 3B) showed two successive
211 inflection points. The first inflection point was related to the presence of a strong acid, i.e.,
212 H_3O^+/H_2O from HCl (Eq.(4)). The second one was related to a weak acid, i.e., NH_3^+/NH_2 groups
213 in CH (Eq.(5)). Cat-CH H_2O showed only one inflection point related to Eq.(5) (see Figure A. 3).
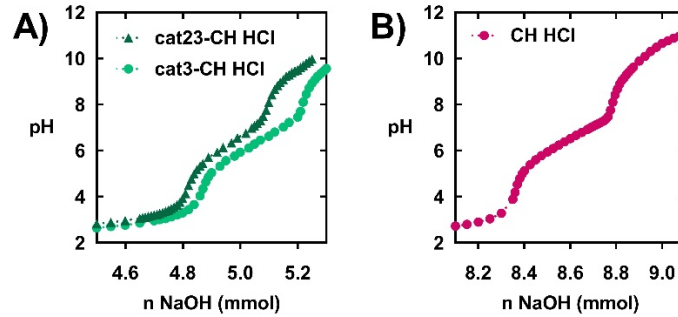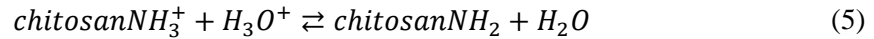

214

215 Figure 3: Titration of cat3-CH (circles), cat23-CH (triangles) (A) and CH (B) in 50 mM HCl with NaOH.
216 Curves have been cropped to emphasize on inflection points.

$$H_3O^+ + HO^- \rightleftarrows 2H_2O \tag{4}$$

$$chitosanNH_3^+ + H_3O^+ \rightleftarrows chitosanNH_2 + H_2O \tag{5}$$

217 To reach equivalence of Eq.(5), we introduced nNaOH=0.35mmol for cat3-CH HCl and
218 nNaOH=0.31mmol for cat3-CH H_2O (see Table A. 1). This confirmed that adding HCl increased
219 the ratio of NH_3^+ versus NH_2 in cat-CH, as known as ionization degree. A lower amount of NaOH
220 was needed for cat23-CH (nNaOH=0.29mmol in both systems). Indeed, the lower proportion of
221 amino groups in highly grafted cat-CH required fewer H+ to ionize it fully.

222 Table 1: pKa calculated through Eq.(2) for cat3-CH, cat23-CH and CH titrated in HCl. Mean of n=2

Polymer	Cat3-CH	Cat23-CH	CH
pKa	6.28	6.26	6.44

223

224   We considered NH_3^+ to be strongly predominant over NH_2 after the first equivalence. We calculated
225   the pKas at the second inflection point with Eq.(2). The pKa of 6.44 for chitosan matched
226   previously obtained results [37] (Table 1). The pKa of cat-CH was 6.27 ± 0.01 and was not
227   influenced by χ. This validated that we can physically crosslink cat-CH with SHC to create
228   thermosensitive hydrogels.

3.1.3. Stability of cat-CH Solutions

230   Cat-CHs of all grafting degrees were dissolved at 3.33% (w/v) to be used in further experiments.
231   All cat-CH H_2O solutions left in contact with air turned orange after 24h, the more grafted the
232   darker, and they had formed soft gels due to oxidative crosslinking. In contrast, HCl successfully
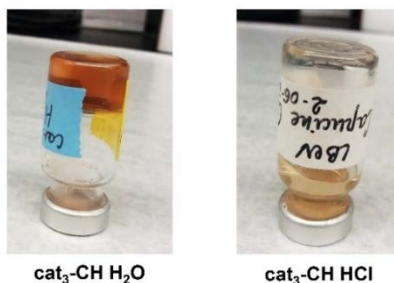233   protected cat groups as cat-CH HCl solutions remained unoxidized (see Figure 4).

cat$_3$-CH H$_2$O   cat$_3$-CH HCl

235   Figure 4: cat-CH solutions in upside down bottles after several months of preservation at 4° C. On the left,
236   cat-CH H_2O is oxidized and has formed a gel, while on the right, cat-CH HCl is still clear and flows

3.2. Cat-CH hydrogels

238   Cat-CH mixed with SHC was able to form hydrogels at 37 °C. All hydrogels were orange after
239   24h, indicating oxidation (see some examples on Figure 5A). Addition of HCl did not prevent
240   oxidation during gelation, because H3O+ from HCl and HCO_3^- from SHC instantaneously reacted
241   together (Eq.(6)). As a result, hydrogels with HCl were as oxidized as hydrogels without HCl.
242   Moreover, starting from SHC80 for cat-CH H_2O and SHC110 for cat-CH HCl, hydrogels had
243   turned opaque within 24h and had released a lot of water.

$$H_3O^+ + HCO_3^- \rightarrow 2H_2O + CO_2 \nearrow \qquad (6)$$
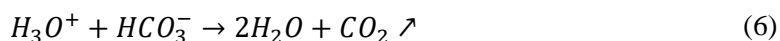
3.2.1. Mechanical properties of hydrogels

246   Unconfined compression tests performed on fully gelled samples (after 24 hours at 37 °C) showed
247   the impact of the composition on the mechanical properties (Figure 5B). SHC concentration had a
248   strong impact on the mechanical behaviour of cat3-CH H_2O/SHC hydrogels. Rigidity increased
249   with SHC concentration, following a bell-shaped curve that reached a maximum at 70 mM SHC
250   (SHC70) (Figure 5B). Further, the hydrogels happened to be more fragile with a lowered
251   toughness; while SHC70 hydrogels withstood compression up to 50% strain, SHC80 hydrogels
252   ruptured below 40% strain (Figure A. 4). The optimum SHC concentration (SHC70) correlates to
253   a stoichiometric ratio between HCO_3^- and the concentration of NH_3^+ in cat-CH. Under that value,
254   there was not enough SHC to interact with NH_3^+ hence gelation was incomplete. Above, the excess
255   SHC that did not escape as CO_2 remained entrapped in the network, impeding the interactions
256   between the CH chains and lowering the mechanical properties.

257   The same trend was observed for cat3-CH HCl/SHC hydrogels, i.e., a bell curve, with a maximum
258   at SHC100. The 30 mM SHC offset between the two conditions (Figure 5B) amounts to the SHC

259 that reacted with HCl before gelation, hence a higher SHC concentration was needed for the system
260 to be in stoichiometric proportions. Increasing SHC further also led to opaque and brittle hydrogels.
261 Surprisingly, the rigidity of the best cat3-CH HCl hydrogels was significantly lower than the
262 rigidity of the best cat3-CH H_2O hydrogels despite their initially higher ionization degree. One
263 possible explanation of this unexpected result is the immediate CO_2 release that we witness while
264 making the cat-CH HCl/SHC pre-gel solutions. The reaction taking place between HCl and SHC
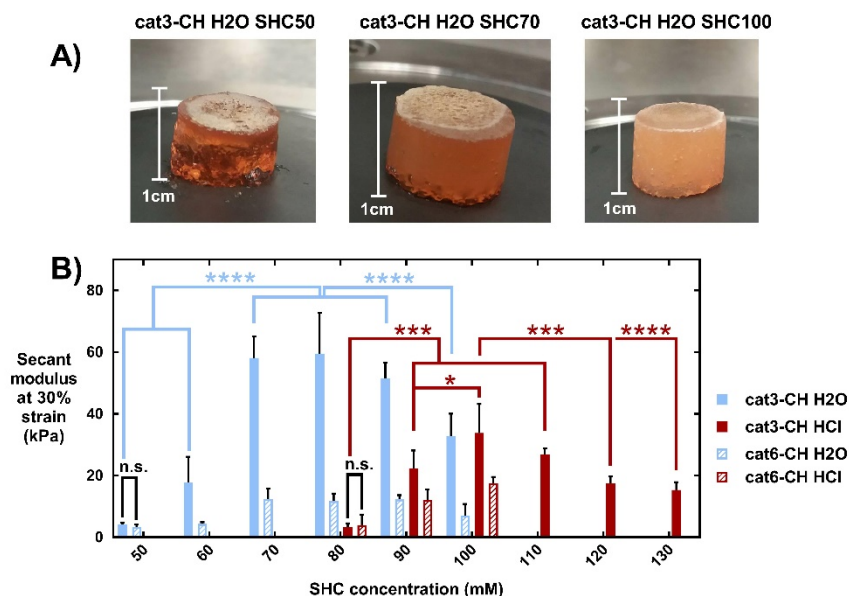265 creates bubbles that could have weakened the network by staying trapped between the chains.

267 Figure 5: A) Cat3-CH H_2O hydrogels with SHC50, SHC70 and SHC100. B) Secant modulus of cat-CH
268 H_2O and cat-CH HCl hydrogels (χ=3% or 6%) as a function of SHC concentration (secant modulus at 30%
269 strain, mean and SD of n=9).

270 Nonetheless, both cat-CH HCl SHC100 and cat-CH H_2O SHC70 showed good mechanical
271 properties with E50%=65kPa and 90 kPa respectively (Figure A. 5). This is lower than for
272 unmodified CH-SHC hydrogels (E50%=140 kPa, data not shown) but much higher than for
273 oxidatively crosslinked cat-CH hydrogels (E <10 kPa [28]). The benefits of physical gelation were
274 clear: mechanical properties of cat3-CH H_2O SHC70 hydrogels met and even surpassed other
275 previously reported systems such as DOPA-CH/Fe3+ hydrogels which break below 40% strain
276 [33].

277 Doubling χ from 3% to 6% drastically decreased the secant modulus, more severely for cat6-CH
278 H_2O hydrogels (around 4.5-fold decrease) than for cat6-CH HCl hydrogels (around two-fold
279 decrease) (Figure 5B). As so, there was no more difference between the best formulations (E=20
280 kPa) which both underwent brittle fracture below 40% deformation (Figure A. 5). This implies that
281 the grafted cat moieties disrupted the network. CH physical crosslinking happens owing to the close
282 proximity of the chains, which results from the charge screening of SHC at room temperature;
283 larger substituents can therefore impede interactions and prevent reaching an optimal spatial
284 organization. Because the molar density of HCA is very close to the molar density of glucosamine
285 (Table A. 2) grafting this large molecule created large branches on the main chain and likely led to
286 irregularities in the hydrogel network. Based on these results, we chose not to make cat-CH
287 hydrogels with a grafting degree higher than 6%.

3.2.2. Thermosensitivity of cat-CH Hydrogels

Temperature ramps were first performed to confirm the thermosensitivity of the hydrogels, then to select the formulations whose behaviour was suitable for mixing cells and injecting them at room temperature prior to in-situ gelation at body temperature. At low temperatures, the storage modulus (G') of all cat3-CH H_2O/SHC hydrogels was low and relatively stable. With increasing temperature, a sharp increase of G' confirmed the thermosensitivity of all formulations (Figure 6A). This increase happened at lower temperatures and was sharper for higher SHC concentrations. The gelation start temperature (GST) was defined at the crossover of G' and G"[38]. All cat3-CH/SHC hydrogels had a GST below 30 °C (Figure 6B) suggesting that all formulations were suited for injection. However, the formulations with the highest SHC had a GST below 22 °C and showed some precipitation at room temperature.

Similarly, gelation time was defined at the crossover of G' and G" during time sweeps. Gelation at 37 °C was below 5 minutes for the hydrogels that showed the best mechanical properties (Figure A. 6A). This is much faster than for other injectable cat-CH systems previously designed [35,39]. However, formulations with less SHC had such a slow increase of G' that it was difficult to differentiate them from one another, hence difficult to highlight the influence of SHC concentration on their gelation kinetics. Therefore, we conducted further time sweeps at 50 °C, which led to a much stronger response with higher G' (Figure A. 6B) and clear differences between the formulations. G' increased faster for cat3-CH HCl/SHC100 than for cat3-CH H_2O/SHC70. Both were much slower to gel than CH/SHC hydrogels, and doubling χ from 3% to 6% significantly tampered the increase of G' (Figure 6C). This can be due either to a slowed gelation or an overall decrease in cohesion, both being direct consequences of the steric hindrance enforced by grafted HCA.

The rheological behaviour of two specific formulations (cat-CH H_2O SHC70 and cat-CH HCl SHC100) was studied more extensively by monitoring their viscosity at 22°C with increasing shear rate, and extruding them through needles. As seen on Figure 6D, their dynamic viscosity at room temperature remained below 3 Pa.s regardless of the shear rate, and they demonstrated a shear-thinning behaviour above 1 s^{-1}. Moreover, we were able to easily extrude them out of a 25G needle (0,455 mm inner diameter). Both of those results corroborated our prediction that these hydrogels were injectable.
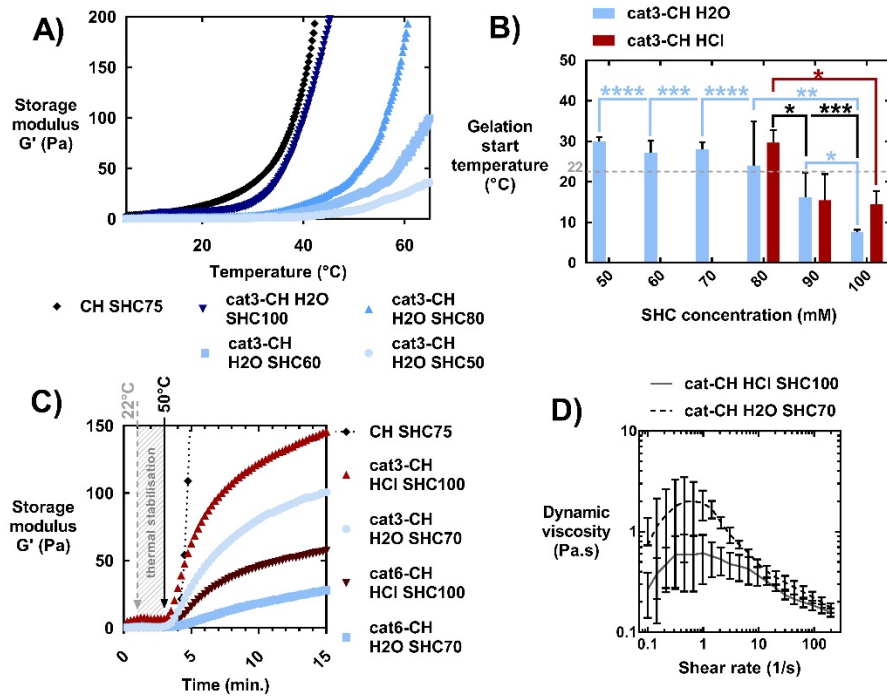
Figure 6: A) Temperature ramps of cat3-CH H_2O/SHC hydrogels as a function of SHC concentration. CH/SHC hydrogel is shown for comparison (mean of n=3, SD not shown). B) Gelation start temperature (G'=G'') for cat3-CH H_2O/SHC hydrogels and cat3-CH HCl/SHC hydrogels. The dashed line marks 22 °C. C) Time sweeps on cat3-CH/SHC hydrogels and cat6-CH/SHC hydrogels. The temperature was set at 22 °C for 1 minute then increased to 50 °C. Reaching 50 °C took approximately 3 minutes, as shown by the black arrow. CH/SHC hydrogel is shown for comparison (mean of n=3, SD not shown). D) Dynamic viscosity of cat3-CH/SHC hydrogels right after mixing.

3.2.3. pH and osmolality of cat-CH hydrogels

We monitored the pH and osmolality of the hydrogels as a first biocompatibility assessment. As expected, cat3-CH H_2O and cat3-CH HCl pH plots followed the same trend with an offset of 30 mM SHC. The pH of the pre-gel solution, just after mixing cat-CH and SHC, was around 6.3 to 6.5, with slightly higher values for the highest SHC concentrations (Figure 7). This, in addition to the low viscosity demonstrated earlier, confirmed that pH sensitive cells or drugs could be mixed to the gel before injection.

The pH changed during gelation at 37 °C; after 24h, the pH of all hydrogels had significantly increased, reaching a pH of 7 to 9 depending on the formulation. While cells can survive in an alkaline environment up to pH9 [40], cell survival tests are mandatory to determine which formulations would be compatible with cell encapsulation.

Osmolality of cat-CH/SHC hydrogel filtrates was in the same range as CH/SHC hydrogels, with about 193 ±11 mOsm/mL [n=6] for cat3-CH/SHC90 compared to 176 [1 for CH/SHC90 (n=3). These values enabled to reach physiological values (around 300 mOsm/mL) when adding cell culture media in the hydrogel, as already demonstrated by our team [10].
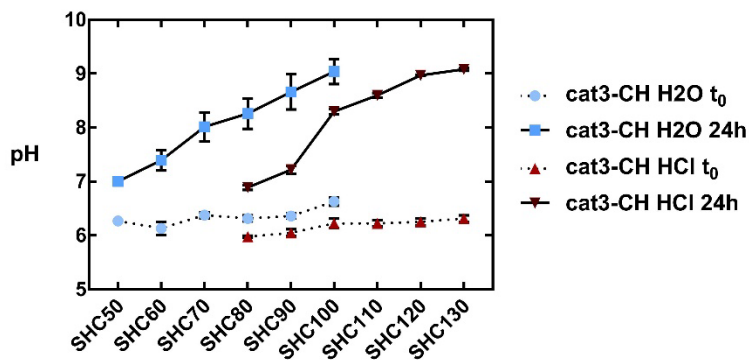
Figure 7: pH of cat3-CH H_2O/SHC (circles and squares) and cat3-CH HCl/SHC (upwards and downwards triangles) hydrogels as a function of SHC concentration. Measures were taken right after mixing (dotted line) and after 24h of gelation at 37 °C (solid line).

3.2.4. *Adhesion of cat-CH Hydrogels*

Adhesion was tested both on organic and inorganic surfaces. We first evaluated inorganic adhesion by measuring the force required to detach the hydrogels from silicate (Figure 8A). As seen on Figure 8B, there was no difference between cat3-CH H_2O/SHC70 and CH/SHC hydrogels while the detachment force was significantly lower for cat3-CH HCl SHC100 which happened to have a lower secant modulus. Data regarding cat-CH without SHC is not shown since these gels were mechanically too weak to yield reliable data. In fact, all hydrogels ruptured at the core, suggesting that in these conditions interfacial adhesion was stronger than gel cohesion. In this experimental setup, mechanical properties were a more significant discriminating factor among hydrogels than adhesive properties. This experiment could not highlight any improvement linked to cat grafting in its oxidized state. This is consistent with previous work reporting that the adhesion of cat on silica is mostly mediated by weak interactions like hydrogen bonding [41] for which cat groups need to be in their non-oxidized state [5].
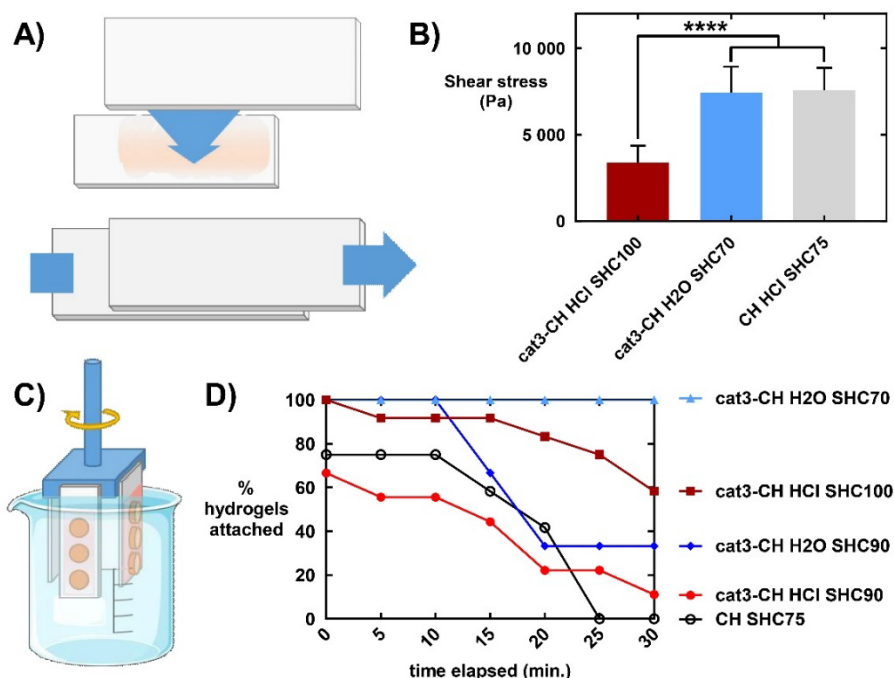
Figure 8: Adhesion tests on inorganic and organic substrates. A) Top: preparation of the samples for shear tests. Bottom: schematic showing the shear test with one of the glass slides being pulled away. B) Detachment force of unmodified CH and different cat3-CH hydrogels (mean and SD of n=6, **** means p <0.001). C) Schematic drawing of wash-off tests. A rotating arm creates shear forces inside a PBS bath (37 °C). Moulded hydrogels are stuck on pig tissue strips, which are glued to the glass slides with cyanoacrylate. D) Percentage of hydrogels still attached to pig mucosa as a function of time, with motor speed increasing from 25 rpm to 250 rpm, at 25 rpm/5 min.

Organic adhesion, on the other hand, was assessed after 24h of in-situ gelation on pig intestines. We counted the numbers of hydrogels that detached under stirring with time and increasing rotor speed in a PBS bath at 37 °C (Figure 8C). In these conditions, cat3-CH H_2O/SHC70 and cat3-CH HCl/SHC100 hydrogels showed higher adhesion than CH/SHC hydrogels (Figure 8D). After 25 minutes (150 rpm), all CH/SHC hydrogels had detached while all cat3-CH H_2O/SHC70 hydrogels were still adherent. As already discussed, we can link this improved adhesion to the in-situ formation of covalent bonds between quinones and the mucosal tissue. Compared to the toughest hydrogels, weaker formulations such as H_2O/SHC90 (too much SHC) or HCl/SHC90 (not enough SHC) showed lower adhesion. Thus, we believe that adhesive properties and mechanical properties, hence the combination of catechol grafting and physical gelation both played a role in increasing bioadhesion.

Bioadhesion is always challenging to compare between studies due to both a shortage in available standardized procedures to measure it and the great variability inherent to those experimental setups. In our experiment, cat-CH/SHC hydrogels held to the animal tissue longer than CH/SHC hydrogels despite our stirring rates being much higher than for previously reported data [39]. This is very encouraging in regard to the ability of our hydrogels to resist shear forces in-vivo. Future work could explore the adhesive properties of these hydrogels in a shorter time frame closer to in-vivo conditions.

Mechanical properties and rapid gelation are also key parameters to ensure good retention at the target tissue. In this work, we showed that, in accordance to our hypothesis, it is possible to form cat-CH hydrogels using SHC. Their gelation time at 37°C was under five minutes while cat-CH oxidation is a much slower process [42]. Even though we could not demonstrate quantitatively our

388 hypothesis, we made the following assumption: the chains rapidly setting into a rigid conformation
389 impeded their further mobility and therefore limited further oxidative crosslinking. This is
390 supported by our results regarding mechanical properties and bioadhesive properties, greatly
391 improved compared to previously reported systems. Physical gelation provides advantages
392 compared to other gelation routes that have been explored to avoid using the cat groups as
393 crosslinkers. Cat-CH gels have been synthesized in previous studies using metal/ion coordination
394 [43–45], genipin [21,45], or pluronic [35]. Yet, most of these hydrogels still have poor mechanical
395 resistance [46] and are usually not injectable [33,43]. Genipin-based gelation takes more than 1h
396 to occur [39] while a short gelation time is mandatory for an injectable gel to adhere to the tissues
397 without leaking.

398 Titration against NaOH showed that HCl did improve the ionization state of CH, although this did
399 not result in improved mechanical properties for the hydrogels. In fact, HCl and SHC reacted
400 together prior to gelation, preventing HCl to protect the cat groups against oxidation, and releasing
401 CO_2 bubbles that possibly disrupted the network. In the mussel, mfp-6 is thought to play a major
402 role in lowering the pH and acting as a reducing agent thanks to its thiol residues [47]. Other
403 strategies to avoid catechol-to-quinone oxidation during preparation include the co-grafting of
404 thiourea groups to mimic the role of mfp-6 [48] or the use of nitro-dopamine as a cat bearing
405 molecule to increase its resistance to auto oxidation [27].

4. Conclusion

407 Combining cat-CH and SHC allowed us to fabricate bioadhesive hydrogels that are injectable
408 thanks to their thermosensitivity and their shear-thinning behaviour. The cat-CH/SHC hydrogels
409 showed a quick gelation at 37°C and reached a high secant modulus with time, improving overall
410 adhesion. Adding HCl did not prevent oxidation of catechols. Nonetheless, the good gelation
411 kinetics, the high mechanical cohesion and the excellent bioadhesion hint towards a successful
412 decrease in oxidative crosslinking.

413 This technology has many advantages, namely a faster gelation at body temperature than previously
414 reported systems, good cohesion and toughness, increased bioadhesion, and a pH and osmolality
415 close to physiological values. All those design features are essential in the design of injectable
416 adhesive vehicles with good anchorage to the target tissues for drug delivery and cell encapsulation.
417 To the best of our knowledge, so far no CH hydrogel has shown them all at once. Further
418 biocompatibility tests will be required to confirm the absence of toxic effect on surrounding tissues
419 and the prospected compatibility with cell encapsulation for cell therapy applications.

5. Acknowledgements

6. References

426 [1] J. Li, D.J. Mooney, Designing hydrogels for controlled drug delivery, Nat. Rev. Mater. 1 (2016)
427   16071. https://doi.org/10.1038/natrevmats.2016.71.

428 [2] K.H. Bae, L.-S. Wang, M. Kurisawa, Injectable biodegradable hydrogels: progress and challenges,
429   J. Mater. Chem. B. 1 (2013) 5371. https://doi.org/10.1039/c3tb20940g.

430 [3] J.D. Smart, The basics and underlying mechanisms of mucoadhesion, Adv. Drug Deliv. Rev. 57
431   (2005) 1556–1568. https://doi.org/10.1016/j.addr.2005.07.001.

432 [4]   J. Hurler, N. Škalko-Basnet, Potentials of Chitosan-Based Delivery Systems in Wound Therapy:
433   Bioadhesion Study, J. Funct. Biomater. 3 (2012) 37–48. https://doi.org/10.3390/jfb3010037.

434 [5]   H. Lee, N.F. Scherer, P.B. Messersmith, Single-molecule mechanics of mussel adhesion, Proc. Natl.
435   Acad. Sci. 103 (2006) 12999–13003. https://doi.org/10.1073/pnas.0605552103.

436 [6]   F. Croisier, C. Jérôme, Chitosan-based biomaterials for tissue engineering, Eur. Polym. J. 49 (2013)
437   780–792. https://doi.org/10.1016/j.eurpolymj.2012.12.009.

438 [7]   V. Grabovac, D. Guggi, A. Bernkop-Schnürch, Comparison of the mucoadhesive properties of
439   various   polymers,   Adv.   Drug   Deliv.   Rev.   57   (2005)   1713–1723.
440   https://doi.org/10.1016/j.addr.2005.07.006.

441 [8]   A. Chenite, C. Chaput, D. Wang, C. Combes, M. Buschmann, C.D. Hoemann, J.C. Leroux, B.L.
442   Atkinson, F. Binette, A. Selmani, Novel injectable neutral solutions of chitosan form biodegradable
443   gels in situ, Biomaterials. 21 (2000) 2155–2161. https://doi.org/10.1016/S0142-9612(00)00116-2.

444 [9]   H.Y. Zhou, L.J. Jiang, P.P. Cao, J.B. Li, X.G. Chen, Glycerophosphate-based chitosan
445   thermosensitive hydrogels and their biomedical applications, Carbohydr. Polym. 117 (2015) 524–
446   536. https://doi.org/10.1016/j.carbpol.2014.09.094.

447 [10] C. Ceccaldi, E. Assaad, E. Hui, M. Buccionyte, A. Adoungotchodo, S. Lerouge, Optimization of
448   Injectable Thermosensitive Scaffolds with Enhanced Mechanical Properties for Cell Therapy,
449   Macromol. Biosci. 17 (2017) 1600435. https://doi.org/10.1002/mabi.201600435.

450 [11] D. Kültz, Chapter 12 Osmotic regulation of DNA activity and the cell cycle, in: Cell Mol. Response
451   to Stress, Elsevier, 2000: pp. 157–179. https://doi.org/10.1016/S1568-1254(00)80014-5.

452 [12] M. Lavertu, D. Filion, M. Buschmann, Heat-induced transfer of protons from chitosan to glycerol
453   phosphate produces chitosan precipitation and gelation, Biomacromolecules. 9 (2008) 640–650.
454   https://doi.org/10.1021/bm700745d.

455 [13] L. Liu, X. Tang, Y. Wang, S. Guo, Smart gelation of chitosan solution in the presence of NaHCO 3
456   for   injectable   drug   delivery   system,   Int.   J.   Pharm.   414   (2011)   6–15.
457   https://doi.org/10.1016/j.ijpharm.2011.04.052.

458 [14] E. Assaad, M. Maire, S. Lerouge, Injectable thermosensitive chitosan hydrogels with controlled
459   gelation kinetics and enhanced mechanical resistance, Carbohydr. Polym. 130 (2015) 87–96.
460   https://doi.org/10.1016/j.carbpol.2015.04.063.

461 [15] Q. Guo, J. Chen, J. Wang, H. Zeng, J. Yu, Recent progress in synthesis and application of mussel-
462   inspired adhesives, Nanoscale. (2020). https://doi.org/10.1039/C9NR09780E.

463 [16] B.P. Lee, P.B. Messersmith, J.N. Israelachvili, J.H. Waite, Mussel-Inspired Adhesives and Coatings,
464   Annu. Rev. Mater. Res. 41 (2011) 99–132. https://doi.org/10.1146/annurev-matsci-062910-100429.

465 [17] L. Duan, Q. Yuan, H. Xiang, X. Yang, L. Liu, J. Li, Fabrication and characterization of a novel
466   collagen-catechol   hydrogel,   J.   Biomater.   Appl.   32   (2018)   862–870.
467   https://doi.org/10.1177/0885328217747125.

468 [18] C. Fan, J. Fu, W. Zhu, D.-A. Wang, A mussel-inspired double-crosslinked tissue adhesive intended
469   for   internal   medical   use,   Acta   Biomater.   33   (2016)   51–63.
470   https://doi.org/10.1016/J.ACTBIO.2016.02.003.

471 [19] S. Hong, K. Yang, B. Kang, C. Lee, I.T. Song, E. Byun, K.I. Park, S.-W.W. Cho, H. Lee, Hyaluronic
472   acid catechol: A biopolymer exhibiting a pH-dependent adhesive or cohesive property for human
473   neural   stem   cell   engineering,   Adv.   Funct.   Mater.   23   (2013)   1774–1780.
474   https://doi.org/10.1002/adfm.201202365.

475 [20] K. Kim, K. Kim, J.H. Ryu, H. Lee, Chitosan-catechol: A polymer with long-lasting mucoadhesive
476   properties, Biomaterials. 52 (2015) 161–170. https://doi.org/10.1016/j.biomaterials.2015.02.010.

477   [21]   J. Xu, G.M. Soliman, J. Barralet, M. Cerruti, Mollusk glue inspired mucoadhesives for biomedical
478   applications, Langmuir. 28 (2012) 14010–14017. https://doi.org/10.1021/la3025414.

479   [22]   G.M. Soliman, Y.L. Zhang, G. Merle, M. Cerruti, J. Barralet, Hydrocaffeic acid-chitosan
480   nanoparticles with enhanced stability, mucoadhesion and permeation properties, Eur. J. Pharm.
481   Biopharm. 88 (2014) 1026–1037. https://doi.org/10.1016/j.ejpb.2014.09.003.

482   [23]   A.H. Hofman, I.A. van Hees, J. Yang, M. Kamperman, Bioinspired Underwater Adhesives by Using
483   the   Supramolecular   Toolbox,   Adv.   Mater.   30   (2018)   1704640.
484   https://doi.org/10.1002/adma.201704640.

485   [24]   B.K. Ahn, Perspectives on Mussel-Inspired Wet Adhesion, J. Am. Chem. Soc. 139 (2017) 10166–
486   10171. https://doi.org/10.1021/jacs.6b13149.

487   [25]   J. Yang, V. Saggiomo, A.H. Velders, M.A. Cohen Stuart, M. Kamperman, Reaction Pathways in
488   Catechol/Primary Amine Mixtures: A Window on Crosslinking Chemistry, PLoS One. 11 (2016)
489   e0166490. https://doi.org/10.1371/journal.pone.0166490.

490   [26]   G.P. Maier, C.M. Bernt, A. Butler, Catechol oxidation: considerations in the design of wet adhesive
491   materials, Biomater. Sci. 6 (2018). https://doi.org/10.1039/c7bm00884h.

492   [27]   P. Zhao, K. Wei, Q. Feng, H. Chen, D.S.H. Wong, X. Chen, C.C. Wu, L. Bian, Mussel-mimetic
493   hydrogels with defined cross-linkers achieved: Via controlled catechol dimerization exhibiting tough
494   adhesion   for   wet   biological   tissues,   Chem.   Commun.   53   (2017)   12000–12003.
495   https://doi.org/10.1039/c7cc07215e.

496   [28]   E. Byun, J.H. Ryu, H. Lee, Catalyst-mediated yet catalyst-free hydrogels formed by interfacial
497   chemical activation., Chem. Commun. 50 (2014) 2869–72. https://doi.org/10.1039/c3cc49043b.

498   [29]   Y. Alinejad, A. Adoungotchodo, E. Hui, F. Zehtabi, S. Lerouge, An injectable chitosan/chondroitin
499   sulfate hydrogel with tunable mechanical properties for cell therapy/tissue engineering, Int. J. Biol.
500   Macromol. 113 (2018) 132–141. https://doi.org/10.1016/J.IJBIOMAC.2018.02.069.

501   [30]   M. Lavertu, Z. Xia, A.N. Serreqi, M. Berrada, A. Rodrigues, D. Wang, M.D. Buschmann, A. Gupta,
502   A validated 1H NMR method for the determination of the degree of deacetylation of chitosan, J.
503   Pharm. Biomed. Anal. 32 (2003) 1149–1158. https://doi.org/10.1016/S0731-7085(03)00155-9.

504   [31]   K. Kim, J.H. Ryu, Y. Lee, H. Lee, Bio-inspired catechol conjugation converts water-insoluble
505   chitosan into a highly water-soluble, adhesive chitosan derivative, Biomater. Sci. 1 (2013) 783–790.
506   https://doi.org/Doi 10.1039/C3bm00004d.

507   [32]   C.M. Lehr, J.A. Bouwstra, E.H. Schacht, H.E. Junginger, In vitro evaluation of mucoadhesive
508   properties of chitosan and some other natural polymers, Int. J. Pharm. 78 (1992) 43–48.
509   https://doi.org/10.1016/0378-5173(92)90353-4.

510   [33]   M. Krogsgaard, M.R. Hansen, H. Birkedal, Metals and polymers in the mix: fine-tuning the
511   mechanical properties and color of self-healing mussel-inspired hydrogels, J. Mater. Chem. B. 2
512   (2014) 8292–8297. https://doi.org/10.1039/C4TB01503G.

513   [34]   J.M. Lee, J.H. Ryu, E.A. Kim, S. Jo, B.-S. Kim, H. Lee, G.-I. Im, Adhesive barrier/directional
514   controlled release for cartilage repair by endogenous progenitor cell recruitment., Biomaterials. 39
515   (2015) 173–81. https://doi.org/10.1016/j.biomaterials.2014.11.006.

516   [35]   J.H. Ryu, Y. Lee, W.H. Kong, T.G. Kim, T.G. Park, H. Lee, Catechol-functionalized
517   chitosan/pluronic hydrogels for tissue adhesives and hemostatic materials, Biomacromolecules. 12
518   (2011) 2653–2659. https://doi.org/10.1021/bm200464x.

519   [36]   Y. Liang, X. Zhao, P.X. Ma, B. Guo, Y. Du, X. Han, pH-responsive injectable hydrogels with
520   mucosal adhesiveness based on chitosan-grafted-dihydrocaffeic acid and oxidized pullulan for
521   localized   drug   delivery,   J.   Colloid   Interface   Sci.   536   (2019)   224–234.

522   https://doi.org/10.1016/J.JCIS.2018.10.056.

523   [37]   J.W. Park, K.-H. Choi, Acid-Base Equilibria and Related Properties of Chitosan, Bull. Korean Chem.
524   Soc. 4 (1983) 68–72.

525   [38]   H.H. Winter, F. Chambon, Analysis of Linear Viscoelasticity of a Crosslinking Polymer at the Gel
526   Point, J. Rheol. (N. Y. N. Y). 30 (1986) 367–382. https://doi.org/10.1122/1.549853.

527   [39]   J. Xu, S. Strandman, J.X.X. Zhu, J. Barralet, M. Cerruti, Genipin-crosslinked catechol-chitosan
528   mucoadhesive hydrogels for buccal drug delivery, Biomaterials. 37 (2015) 395–404.
529   https://doi.org/10.1016/j.biomaterials.2014.10.024.

530   [40]   C.R. Kruse, M. Singh, S. Targosinski, I. Sinha, J.A. Sørensen, E. Eriksson, K. Nuutila, The effect of
531   pH on cell viability, cell migration, cell proliferation, wound closure, and wound reepithelialization:
532   In vitro and in vivo study, Wound Repair Regen. 25 (2017) 260–269.
533   https://doi.org/10.1111/wrr.12526.

534   [41]   J. Saiz-Poseu, J. Mancebo-Aracil, F. Nador, F. Busqué, D. Ruiz-Molina, The Chemistry behind
535   Catechol-Based Adhesion, Angew. Chemie Int. Ed. 58 (2019) 696–714.
536   https://doi.org/10.1002/anie.201801063.

537   [42]   A.R. Narkar, E. Cannon, H. Yildirim-Alicea, K. Ahn, Catechol-Functionalized Chitosan: Optimized
538   Preparation Method and Its Interaction with Mucin, Langmuir. 35 (2019) 16013–16023.
539   https://doi.org/10.1021/acs.langmuir.9b02030.

540   [43]   P.S. Yavvari, A. Srivastava, Robust, self-healing hydrogels synthesised from catechol rich polymers,
541   J. Mater. Chem. B. 3 (2015) 899–910. https://doi.org/10.1039/c4tb01307g.

542   [44]   A. Ghadban, A.S. Ahmed, Y. Ping, R. Ramos, N. Arfin, B. Cantaert, R. V. Ramanujan, A. Miserez,
543   Bioinspired pH and magnetic responsive catechol-functionalized chitosan hydrogels with tunable
544   elastic properties, Chem. Commun. 52 (2016) 697–700. https://doi.org/10.1039/C5CC08617E.

545   [45]   S. Azevedo, A.M.S. Costa, A. Andersen, I.S. Choi, H. Birkedal, J.F. Mano, Bioinspired Ultratough
546   Hydrogel with Fast Recovery, Self-Healing, Injectability and Cytocompatibility, Adv. Mater. 29
547   (2017) 1700759. https://doi.org/10.1002/adma.201700759.

548   [46]   J.H. Ryu, S. Hong, H. Lee, Bio-inspired adhesive catechol-conjugated chitosan for biomedical
549   applications: A mini review, Acta Biomater. 27 (2015) 101–115.
550   https://doi.org/10.1016/j.actbio.2015.08.043.

551   [47]   J. Yu, W. Wei, E. Danner, R.K. Ashley, J.N. Israelachvili, J.H. Waite, Mussel protein adhesion
552   depends on interprotein thiol-mediated redox modulation, Nat. Chem. Biol. 7 (2011) 588–590.
553   https://doi.org/10.1038/nchembio.630.

554   [48]   Y.J. Xu, K. Wei, P. Zhao, Q. Feng, C.K.K. Choi, L. Bian, Preserving the adhesion of catechol-
555   conjugated hydrogels by thiourea-quinone coupling, Biomater. Sci. 4 (2016) 1726–1730.
556   https://doi.org/10.1039/c6bm00434b.

557

558 # Appendix A: Supplementary data

559

560 Table A. 1: NaOH at equivalence for cat3-CH, cat23-CH and CH in either H_2O or HCl

Solubilisation	H_2O		HCl		
Polymer	**Cat3-CH**	**Cat23-CH**	**Cat3-CH**	**Cat23-CH**	**CH**
First inflection point	N/A	N/A	4.87	4.82	8.15
Second inflection point	0.32	0.29	5.23	5.11	8.57
Delta n	N/A	N/A	0.36	0.29	0.42

561

562 Table A. 2: Physical properties of caffeic acid and glucosamine

	Caffeic Acid	**Glucosamine**
Density (g/cm3)	1.48	1.56
Molecular weight (g/mol)	180.2	179.2
Molar density (mol/cm3)	121.9	114.6

563

564

$$\chi = \frac{C_{cat} * (dd_A * M_{Glu} + (1 - dd_A * M_{AcGlu})}{C_{w,cat-CH} - M_{HCA} * C_{cat}} \qquad (A.1)$$

- ddA: deacetylation degree of CH
- M_{Glu}: molar mass of the CH glucosamine monomer (161 g/mol)
- M_{AcGlu}: molar mass of CH acetyl-glucosamine monomer (203 g/mol)
- M_{HCA}: molar mass of HCA, C_w is the mass concentration of cat-CH
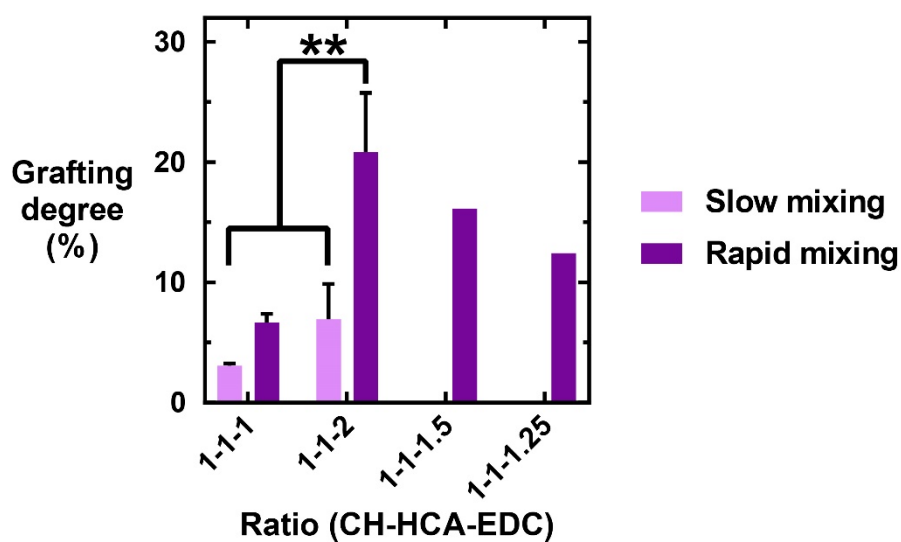- [catechol]: molar concentration of catechol found through the calibration curve.

565

566

567

568 Figure A. 1: Grafting degree of chitosan with catechol measured by UV-Visible Spectrometry. Two
569 conditions are tested, i.e. the ratio between reagents and the mixing speed. Statistical analysis indicate a
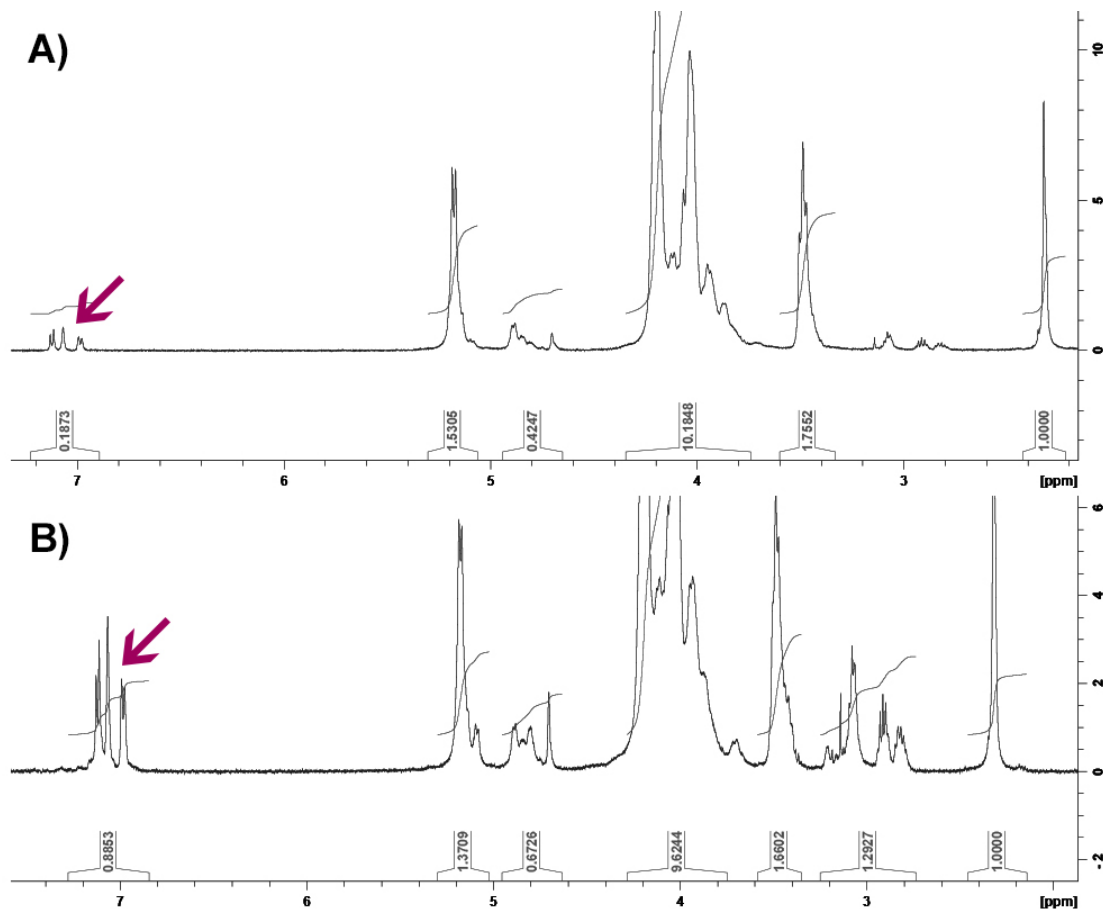570 strong synergy between an excess of EDC and a fast mixing during the reaction.

571

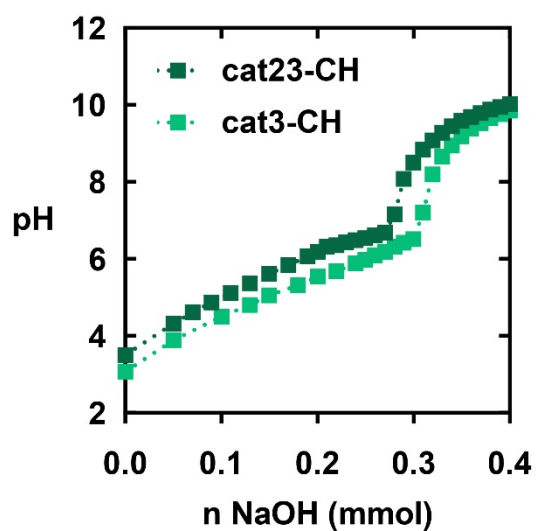572 Figure A. 2: NMR[1]H spectra of A) cat3-CH and B) cat20-CH.

573

Figure A. 3: Titration of cat3-CH H_2O and cat23-CH H_2O with NaOH shows only one inflection point related to amino groups of chitosan. Because catechol-chitosan is not in its full ionization state, it is not possible to calculate the pKa.
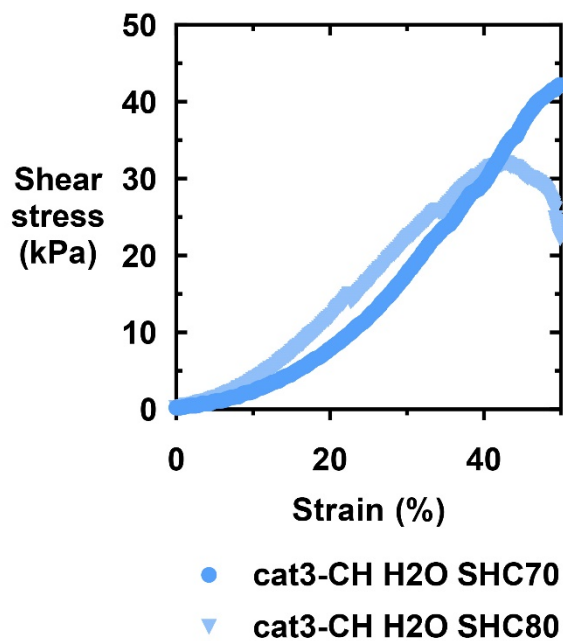
577

578

Figure A. 4: Stress-strain curves for cat3-CH H_2O/SHC70 and cat3-CH H_2O/SHC80. While SHC70 could be stressed up to 50% strain, SHC80 hydrogels broke before 40% strain in a brittle fracture.
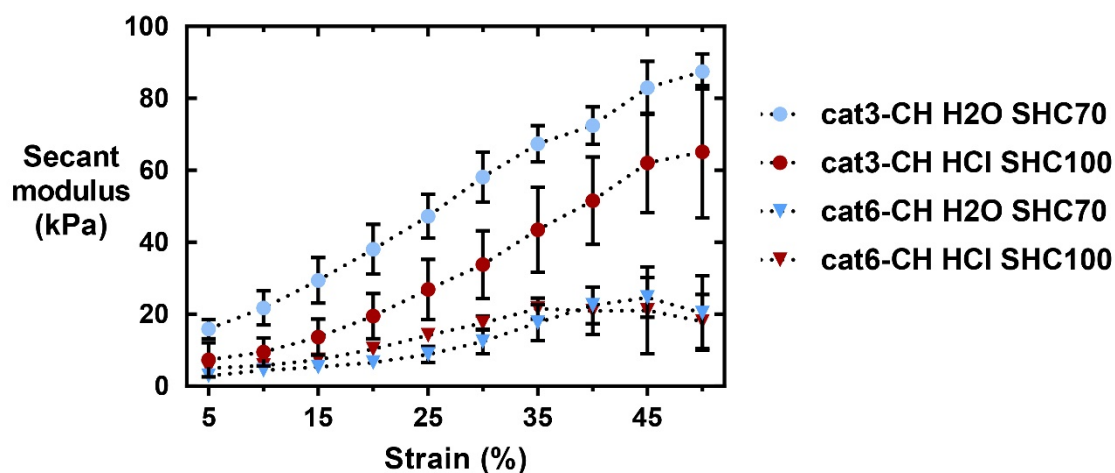
581

Figure A. 5: Comparison of secant modulus of cat3-CH H_2O/SHC70, cat3-CH HCl/SHC100, cat6-CH H_2O/SHC70 and cat6-CH HCl/SHC100 (mean and SD of n=9) at different strains. Catechol grafting degree has a significant impact on mechanical properties.
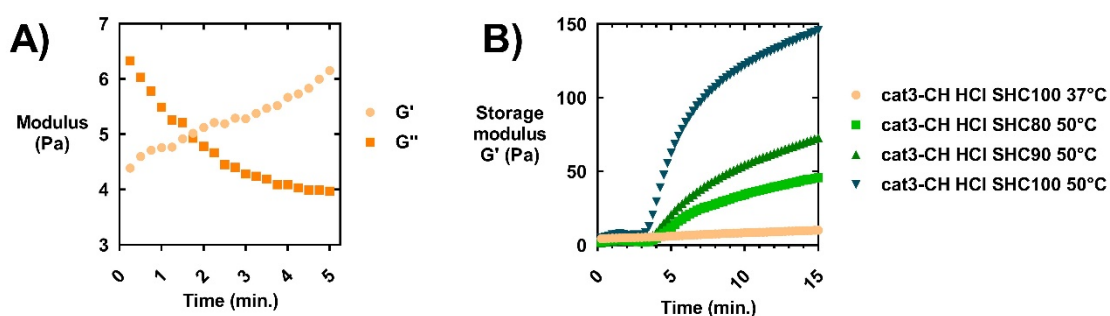
585

586

Figure A. 6: A) Time sweep: 5 minutes at 37°C for cat3-CH HCl/SHC100 B) Time sweeps: 1 min at 22°C, followed by an increase at 37°C for cat3-CH HCl/SHC100 or at 50°C for cat3-CH HCl/SHC80-90-100.

589

590

<h1 align="center">Vitae</h1>

Capucine Guyot

Capucine Guyot is a PhD student at Ecole de Technologie Supérieure in Dr. Lerouge's lab since 2016, under the co-supervision of Dr. Cerruti. She graduated from Ecole Centrale de Lyon, France with a bachelor in Materials Engineering in 2015 and a master's in biomedical engineering in 2016. She has already presented her work in several conferences about biomaterials including the 2018 Society for Biomaterials meeting and the 2019 Canadian Biomaterials Society meeting.

Marta Cerruti

Marta Cerruti is Associate Professor in Materials Engineering at McGill University. Since 2011, she is Canada Research Chair (Tier 2) in Bio-synthetic interfaces. Her research focuses on controlling interactions between material surfaces and biomolecules. She is a member of the College of New Scholars, Artists, and Scientists of the Royal Society of Canada and was one of the Young Scientists at the World Economic Forum in 2017 and 2018. She published 90 papers on journals including JACS, Advanced Materials, Nanoscale, etc, and was interviewed by CBC radio twice for her work on arterial and heart valve calcification.

615 **Sophie Lerouge**

616

617 Sophie Lerouge is full professor at Ecole de technologie supérieure (ÉTS) and researcher at the
618 CHUM research center (CRCHUM) in Montréal. International Fellow in Biomaterials science and
619 engineering since 2016, she is also board member of the Canadian Biomaterials Society of which
620 she was President in 2018–2019. Through her multidisciplinary approach at the frontier between
621 material science and cell biology, she has been developing coatings, implants and injectable
622 hydrogels for tissue regeneration and cell therapy. Her work has led to more than 80 peer review
623 papers, as well as several patents, innovations and research awards.

624